EZH2 and histone deacetylase inhibitors induce apoptosis in triple negative breast cancer cells by differentially increasing H3 Lys^{27} acetylation in the *BIM* gene promoter and enhancers

JULIA P. HUANG and KUN LING

Department of Biochemistry and Molecular Biology, Mayo Clinic College of Medicine, Rochester, MN 55905, USA

Received November 6, 2016; Accepted March 30, 2017

DOI: 10.3892/ol.2017.6912

Abstract. Enhancer of zeste homolog 2 (EZH2), a subunit of polycomb repressive complex 2, is a histone methyltransferase and is considered to work cooperatively with histone deacetylases (HDACs) in the same protein complex to mediate gene transcription repression by increasing histone H3 Lys^{27} trimethylation (H3K27me3), in particular in the nucleosome (s). EZH2 is overexpressed in numerous types of cancer, including triple negative breast cancer (TNBC), a subtype of breast cancer, which there are no effective treatment options for. Thus, inhibition of EZH2 may be harnessed for targeted therapy of this disease. The present study demonstrated that co-treatment with an EZH2 inhibitor and a HDAC inhibitor additively induced apoptosis in two TNBC cell lines, namely MDA-MB-231 and MDA-MB-436. The increased rate of cell death was associated with an elevation of B cell lymphoma-2 like 11 (BIM) expression level, a pro-apoptotic protein at the protein and mRNA expression levels in these two cell lines. The expression of forkhead box O1 (FOXO1), a known upstream transcriptional activator of *BIM*, was upregulated in both cell lines by the HDAC inhibitor, and the effect was more pronounced in MDA-MB-436 cells with higher phosphorylation levels of protein kinase B, a negative regulator of FOXO1, compared with MDA-MB-231 cells. Conversely, FOXO1 expression was inhibited following treatment with the EZH2 inhibitor, suggesting that EZH2 and HDAC inhibitors induced BIM expression via a FOXO1-independent mechanism. The present study further revealed that the EZH2 inhibitor, but not the HDAC inhibitor, induced high levels of H3K27 acetylation (H3K27ac) in the *BIM* promoter. By contrast, compared with the effect of the EZH2 inhibitor, HDAC inhibitor treatment resulted in an increase in H3K27ac at two *BIM* enhancers. Collectively, the results of the present study indicated that EZH2 and HDACs act differentially on H3K27ac levels in the nucleosome at the promoter and enhancer regions of the *BIM* gene. Through the upregulation of BIM, co-treatment with EZH2 and HDAC inhibitors had a pronounced therapeutic effect on TNBC cells, suggesting that co-targeting EZH2 and HDAC proteins represents a viable therapeutic option for the treatment of TNBC.

Correspondence to: Dr Kun Ling, Department of Biochemistry and Molecular Biology, Mayo Clinic College of Medicine, 200 First Street Southwest, Rochester, MN 55905, USA
E-mail: ling.kun@mayo.edu

Key words: enhancer of zeste 2 polycomb repressive complex 2 subunit, histone deacetylases, B cell lymphoma-2 like 11, forkhead box O1, histone H3 Lys^{27} trimethylation, histone H3 Lys^{27} acetylation, triple negative breast cancer, chemotherapy

Introduction

Breast cancer is the most prevalent type of cancer in females (1). There are >200,000 new cases each year in the USA, and the number is not decreasing (2). In total, >12% of females are diagnosed with breast cancer in their lifetime. In addition to local treatments, including surgery and radiation therapy, breast cancer patients are often systematically treated with hormone therapy, chemotherapy or targeted therapy (3). The biomarkers most commonly used to guide the choice of treatment are estrogen receptor (ER), progesterone receptor (PR) and human epidermal growth factor receptor 2 (HER2). For example, ER- and/or PR-positive breast cancer can be treated with hormone therapy, including tamoxifen, which blocks the binding of estrogen with its cognate receptor. Patients with HER2-positive breast cancer benefit from targeted therapies aimed at blocking HER2 activation (4). However, basal-like triple negative breast cancer (TNBC) does not express any of the above biomarkers, and therefore, it does not respond well to existing systemic therapies and exhibits a high rate of recurrence (5).

Enhancer of zeste homolog 2 (EZH2) belongs to the polycomb group (PcG) protein family (6). Along with other PcG proteins, EZH2 forms a protein complex named polycomb repressive complex 2 (PRC2), which suppresses gene transcription (7). EZH2 is the only enzymatic component of the PRC2 complex that catalyzes histone H3 Lys^{27} trimethylation (H3K27me3), a histone repression mark that mediates close chromatin and epigenetic silencing of genes associated with cell proliferation, migration and invasion.

EZH2 is often overexpressed in numerous types of human cancer, including TNBC (8-10), and has been revealed to promote tumor growth by repressing the expression of tumor-suppressor genes (11-13). Mutations with increased

activity of EZH2 have also been detected in various human types of cancer, including lymphomas (7). Due to aberrant activation of EZH2 in numerous cancer subtypes, EZH2 has been an attractive target for drug development. A few promising small molecule inhibitors of EZH2, including GSK126, have been developed, and their antitumor efficacy has actively been tested in pre-clinical and clinical settings (14,15).

It has been demonstrated that PRC2 components interact with histone deacetylases (HDACs), and EZH2-mediated transcriptional silencing is known to be blocked by HDAC inhibitors (10,16). H3K27me3 induces closed chromatin and gene repression, whereas histone H3 Lys^{27} acetylation (H3K27ac) does the opposite by promoting open chromatin and gene transcription activation (17). It has been hypothesized that HDACs remove the acetyl group from Lys^{27} and make it available for methylation by EZH2, and thereby EZH2 and HDAC proteins work cooperatively to mediate gene silencing by acting on the same nucleosome(s) (8).

EZH2 has been identified as an oncoprotein that is crucial to the growth of TNBC (9); therefore, the present study aimed to determine the cooperative action of EZH2 and HDACs on TNBC by treating TNBC cells with EZH2 or HDAC inhibitors alone or combined. The results of the present study demonstrated that co-treatment with both inhibitors resulted in greater antitumor effects in TNBC, compared with each drug alone.

Materials and methods

Cell lines, cell culture, chemicals and antibodies. The TNBC cell lines MDA-MB-231 and MDA-MB-436 were purchased from the American Type Culture Collection (Manassas, VA, USA) and maintained in Dulbecco's modified Eagle's medium (Thermo Fisher Scientific, Inc., Waltham, MA, USA) supplemented with 10% fetal bovine serum (Thermo Fisher Scientific, Inc.) and 100 μg/ml penicillin-streptomycin-glutamine (Thermo Fisher Scientific, Inc.) at 37˚C with 5% CO_2. The EZH2 inhibitor GSK126 and the HDAC inhibitor LBH589 were purchased from Selleck Chemicals (Houston, TX, USA). Dimethyl sulfoxide (DMSO) was purchased from Sigma-Aldrich; Merck KGaA (Darmstadt, Germany). The antibodies used for western blotting were: Anti-B cell lymphoma-2 like 11 (BIM; (ChemiCon International; Thermo Fisher Scientific, Inc.; catalog no. AB17003; dilution, 1:1,000), anti-poly(ADP-ribose) polymerase (PARP; Cell Signaling Technology, Inc., Danvers, MA, USA; catalog no. 9532; dilution, 1:1,000), anti-forkhead box O1 (FOXO1; Cell Signaling Technology, Inc.; catalog no. 9462L; dilution, 1:1,000), anti-protein kinase B (AKT; Cell Signaling Technology, Inc.; catalog no. 9272; dilution, 1:1,000), anti-phosphorylated (p)-AKT (Ser^{473} phosphorylation; Cell Signaling Technology, Inc.; catalog no. 9471L; dilution, 1:1,000), anti-p27 (Santa Cruz Biotechnology, Inc., Dallas, TX, USA; catalog no. sc-71813, 1:1,000 dilution) and anti-extracellular-signal-related kinase 2 (ERK2; Santa Cruz Biotechnology, Inc.; catalog no. sc-1647; dilution, 1:10,000). The antibodies used for chromatin immunoprecipitation (ChIP) were as follows: Anti-H3K27ac (Abcam, Cambridge, MA, USA; catalog no. ab4729; 5 μg/ChIP assay) and non-specific rabbit immunoglobulin G (IgG; Vector laboratories, Inc., Burlingame, CA, USA; catalog no. I-1000; 5 μg/ChIP assay). Horseradish peroxidase (HRP)-conjugated secondary antibodies (donkey anti-mouse IgG HRP, catalog no. NA931V, dilution 1:5,000; and donkey anti-rabbit IgG HRP, catalog no. NA934V, dilution 1:5,000) for western blotting were purchased from GE Healthcare Life-Sciences (Pittsburgh, PA, USA).

Cell morphology analysis and imaging. MDA-MB-231 and MDA-MB-436 cells ($1x10^5$ cells/well) were plated into 6-well plates at ~20% confluence. At 24 h after plating, incubated at 37˚C (~40% confluence), cells were treated with vehicle (DMSO), GSK126, LBH589 or both GSK126 and LBH589 for 24 h, and morphological images were captured using a DMI3000 B microscope (magnification, x400; Leica Microsystems GmbH, Wetzlar, Germany) from ≥5 random fields.

Analysis of apoptotic cells using fluorescence-activated cell sorting (FACS). Apoptotic cell death (DNA content <2 copy number of unreplicated genome (N) was examined using FACS, as previously described (18). MDA-MB-231 cells were treated with vehicle (DMSO), GSK126, LBH589 or GSK126 and LBH589 for 24 h at 37˚C. Cells were then harvested by centrifugation at 1,000 x g for 5 min. Cells were washed with 1X PBS once, fixated with 70% ethanol on ice for 30 min and stored at -20˚C. Following washing twice with 1X PBS, cells were stained with propidium iodide (PI) in a staining solution, which was supplemented with 20 μg/ml PI (Sigma-Aldrich; Merck KGaA) and 50 μg/ml RNase A (Thermo Fisher Scientific, Inc.), for 30 min at room temperature, and their DNA content profiles were then determined by flow cytometry using FACScan (BD Biosciences, Franklin Lakes, NJ, USA) and apoptotic cells (PI intensity, <2 N) were determined using CellQuest Pro software (version 5.1; BD Biosciences).

Western blot analysis. MDA-MB-231 and MDA-MB-436 cells ($1.5x10^5$ cells/well) were plated into 6-cm dishes at ~30% confluence. At 24 h after plating, incubated at 37˚C (~50% confluence), cells were treated with vehicle (DMSO), GSK126, LBH589 or both GSK126 and LBH589 for 24 h at 37˚C. Cells were then harvested and lysed for 1 h on ice in modified radioimmunoprecipitation assay buffer (1X PBS, 1% Nonidet P-40, 0.1% SDS and 1X protease inhibitor cocktail; Sigma-Aldrich). The protein concentration in the samples was determined using a bicinchoninic acid assay (Thermo Fisher Scientific, Inc.). Equal amounts (80-100 μg protein) of samples were separated using SDS-PAGE (6-10% gels) and transferred onto nitrocellulose membranes. Membranes were pre-blocked with 5% non-fat dry milk (Bio-Rad Laboratories, Inc., Hercules, CA, USA) in 1X TBS for 1 h at room temperature and subsequently incubated overnight at 4˚C with primary antibodies against PARP, BIM, FOXO1, (p)-AKT, AKT or p27. ERK2 was used as a loading control (12). Membranes were washed three times with 1X TBS containing 0.1% Tween-20 and incubated with HRP-conjugated secondary antibodies, goat anti-mouse IgG or anti-rabbit IgG as aforementioned, for 1 h at room temperature. Proteins were detected by chemiluminescence (Thermo Fisher Scientific, Inc.).

RNA extraction and reverse transcription-quantitative polymerase chain reaction (RT-qPCR). MDA-MB-231 and

MDA-MB-436 cells ($2x10^5$ cells/well) were plated into 6-cm dishes. At 24 h after plating, and incubated at 37˚C (~50% confluence), cells were treated with vehicle (DMSO), GSK126, LBH589 or both GSK126 and LBH589 for 24 h at 37˚C. Cells were lysed with TRIzol® reagent (Thermo Fisher Scientific, Inc.) for 10 min at room temperature, and total RNA was extracted following the manufacturer's protocol. cDNA was synthesized using SuperScript II reverse transcriptase (Thermo Fisher Scientific, Inc.) according to the manufacturer's protocol. RT-qPCR was performed using iQ SYBR® Green Supermix (Bio-Rad Laboratories, Inc.) and an iCycler iQ™ Real-Time PCR Detection System (Bio-Rad Laboratories, Inc.), according to the manufacturer's protocol. The PCR cycles (denaturing at 95˚C for 20 sec, annealing at 58˚C for 20 sec and extending at 72˚C for 25 sec) for *BIM* and *GADPDH* genes were between 26 and 30 and between 17 and 19, respectively, in different cell lines and different treatment conditions. The experiments were repeated three times. All the signals were normalized by *GAPDH*, and the $2^{-\Delta\Delta Cq}$ method (19) was used to determine the fold changes in expression of mRNAs. The sequences of the primers used for RT-qPCR were as follows: *BIM* forward, 5'-AGACAGAGCCACAAGCTTCC-3' and reverse, 5'-CAG GCGGACAATGTAACGTA-3'; and *GAPDH* forward, 5'-ACC CACTCCTCCACCTTTGAC-3' and reverse, 5'-TGTTGCTGT AGCCAAATTCGTT-3'.

Analysis of public chromatin immunoprecipitation sequencing (ChIP-seq) data. ChIP-seq signals for the promoter histone mark histone H3 Lys^4 trimethylation (H3K4me3), the enhancer histone mark histone H3 Lys^4 monomethylation (H3K4me1) and transcriptionally active histone mark histone H3 Lys^{27} acetylation (H3K27ac), obtained from LNCaP prostate cancer cells (20), were analyzed and displayed using the University of California at Santa Cruz genome browser (genome.ucsc.edu), as reported previously (21).

ChIP assay. MDA-MB-231 and MDA-MB-436 cells ($3x10^6$ cells/well) were cultured in 10 cm dishes, for 24 h at 37˚C, and treated with vehicle (DMSO), GSK126, LBH589 or both GSK126 and LBH589, for 24 h at 37˚C. Following treatment, ~$5x10^6$ cells in each treatment group were collected and sonicated using a Bioruptor (Diagenode, Inc., Denville, NJ, USA), according to the manufacturer's protocol. ChIP was performed according to a previously described protocol (22). The soluble chromatin was incubated with 5 μg of non-specific control rabbit IgG or anti-H3K27ac antibodies overnight at 4˚C. Immunoprecipitated and input DNA were subjected to reverse cross-linking by incubating at 65˚C overnight. Following treatment with proteinase K at 55˚C for 2 h, DNA was purified using the PureLink Quick PCR Purification kit (Qiagen, Inc., Valencia, CA, USA). ChIP and input samples were analyzed using qPCR using the iQ SYBR® Green Supermix and an iCycler iQ™ Real-Time PCR Detection System (Bio-Rad Laboratories, Inc.), according to manufacturer's protocol. The $2^{-\Delta\Delta Cq}$ method (19) was used to determine the enrichment of ChIP signals. The experiments were performed three times. The sequences of the PCR primers were as follows: *BIM* promoter forward, 5'-GCGGACGTGAGTTTCGGTGTG-3' and reverse, 5'-GGTGCACATCTCTAAATGGGGACGG-3'; *BIM* enhancer-1 forward, 5'-CCCGTTTGTAAGAGGCCA GGC-3' and reverse, 5'-CCTCACTGCTGCCTCGTGGT-3'; and *BIM* enhancer-2 forward, 5'-GGCTATTGGTAAAGG CTAGGTAGCG-3' and reverse 5'-CCGGTACATGCGCTC ACACAG-3'.

Statistical analysis. Experiments were performed in ≥3 replicates unless indicated otherwise. The results are presented as the mean ± standard deviation. Statistical analyses were performed by two-tailed Student's t-test. $P<0.05$ was considered to indicate a statistically significant difference.

Results

EZH2 and HDAC inhibitors induce morphological changes in TNBC cells. To determine the effectiveness of EZH2 and HDAC inhibitors in TNBC, the present study first examined their effects on cell morphology using microscopic analyses. MDA-MB-231 and MDA-MB-436 TNBC cells were treated with vehicle (DMSO), EZH2 inhibitor GSK126 (15 mM), HDAC inhibitor LBH589 (2.5 nM) or both and LBH589 for 24 h. Cells grown under the control condition (0.1% DMSO in complete culture medium) were spindle-like, abundant and well attached to the culture dish. Conversely, following treatment with the above inhibitors, certain cells were detached and became round, a possible indicator of apoptotic cell death (23) (Fig. 1). With the addition of GSK126 alone there was only a slight change, namely a decrease in rigidity and size, in the morphology of the cultured cells. As expected, inhibition of the EZH2 methyl-transferase alone may have little impact on the malignant cells, as it would not address the deacetylation at the H3K27 position (8). With the treatment of LBH589 alone, there was a greater number of cells that were shriveled and no longer attached to the culture dish, compared with mock-treated cells (Fig. 1). The HDAC inhibitor therefore was observed to have a greater impact on tested TNBC cells compared with that of the EZH2 inhibitor alone. Of note, it was revealed that cells treated with both inhibitors were affected the most. A large majority of cells lost their normal morphology and were not able to adhere well to the culture dish (Fig. 1). This distinctly higher level of morphological change, caused by EZH2 and HDAC inhibitors relative to vehicle, suggested an association with an increase in the rate of apoptosis.

Inhibition of EZH2 and HDAC proteins induces apoptotic cell death. To validate the morphological observation, FACS analysis was performed on the cultures of both TNBC cell lines with or without treatment. The cells were stained with PI and analyzed by flow cytometry to determine the amount of DNA in the cells. Cells with a PI intensity <2N were considered apoptotic, as the DNA was fragmented (24). Consistent with the morphological images, there were increasingly higher amounts of fragmented DNA, and thus apoptotic cells, in the cultures treated with GSK126, LBH589 or both, compared with vehicle (Fig. 2A), which is quantitatively presented in Fig. 2B. Specifically, there was a significant increase in the percentage of dead or dying cells in the culture treated with GSK126 and LBH589, compared with mock (DMSO) treatment. Cells treated with the vehicle (DMSO), GSK126 or LBH589 alone exhibited cell death rates of 6.00, 11.57 and

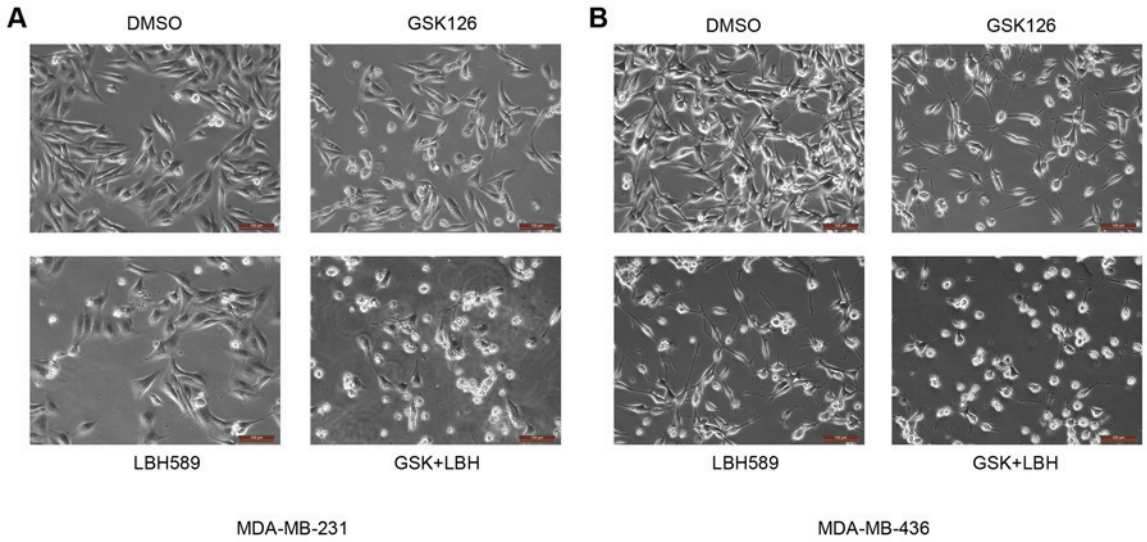

Figure 1. EZH2 and HDAC inhibitors induce morphological changes in MDA-MB231 and MDA-MB-436 cells. (A) MDA-MB-231 and (B) MDA-MB-436 cells were treated with GSK126 (15 μM), LBH589 (2.5 nM) or both for 24 h. Cells growing under normal conditions (DMSO) were spindle-like and attached well to the culture dish. Conversely, following treatment with these inhibitors, certain cells were detached and became round, which is indicative of apoptotic cell death. Scale bars, 100 μm. EZH2, enhancer of zeste 2 polycomb repressive complex 2 subunit; HDAC, histone deacetylase; DMSO, dimethyl sulfoxide; GSK, GSK126; LBH, LBH589.

15.52%, respectively. Cells treated with GSK126 and LBH589 demonstrated a 40.31% apoptotic rate, which was over double the apoptotic level in the culture treated with LBH589 alone (Fig. 2B). The results of simultaneous treatment of GSK126 and LBH589 corroborate the hypothesis that inhibiting methylation by EZH2 and deacetylation by HDACs may induce an additive/synergistic effect in cancer therapy.

Increase in BIM protein expression level induces high levels of apoptosis. As another method to determine apoptosis, the present study evaluated the level of PARP cleavage, an apoptotic marker (25), and a key pro-apoptotic protein, BIM (encoded by a gene termed *BCL2L11*) (26), using western blot analysis. Full-length PARP is a protein involved in DNA repair and chromatin structure formation. During apoptosis, this full-length protein is cleaved into small fragments that are detected as cleaved PARP (25). PARP protein has a unique fragmentation as a result of apoptosis, which allows for convenient detection of the levels of programmed cell death (25). In both MDA-MB-231 and MDA-MB-436 cells treated with either GSK126 or LBH589, cleaved PARP expression level increased inversely to the expression level of uncleaved full-length PARP (Fig. 3). Consistent with the hypothesis of the present study, the combined treatment produced the highest levels of cleaved PARP, therefore resulting in the highest levels of apoptosis detected by FACS analysis (Fig. 2).

The reason for the increased apoptotic levels may be attributed to the overexpression of pro-apoptotic proteins. One such protein, BIM, often serves a key role in apoptosis in all cancer cells (26). Western blotting revealed that treating the cancer cells with GSK126 induced a slight increase in BIM expression. However, following treatment with LBH589, BIM protein expression levels were higher in both cell lines, compared with mock treatment (Fig. 3A and B). Thus, the significant increase in apoptotic levels evident in the cell count analysis (Fig. 2) was in agreement with the immunoblotting results (Fig. 3). The culture treated with both drugs demonstrated the highest levels of BIM expression, again displaying the effectiveness of both inhibitors on malignant cells (Fig. 3).

BIM mRNA expression levels are upregulated by inhibition of EZH2 and HDAC proteins. It was revealed that treatment with EZH2 and HDAC inhibitors induced increased levels of apoptosis in TNBC cells, as demonstrated by the increased levels of BIM protein expression. However, it was unclear whether the promotion of the pro-apoptotic protein and the increased levels of cell death were due to increased mRNA expression of *BIM*. Thus, the effect of GSK126 and LBH589 on the expression levels of *BIM* mRNA was determined by RT-qPCR. Quantitation of the steady-state mRNA expression levels confirmed that EZH2 and HDAC inhibitors upregulated the mRNA expression levels of *BIM* in the MDA-MB-231 and MDA-MB-436 cell lines (Fig. 4). Consistent with the results of the FACS analysis, treatment with GSK126 induced slight increases in *BIM* mRNA expression levels. Also similar to the results presented in Fig. 3, LBH589 induced the second-highest expression levels of *BIM* mRNA (Fig. 4). Finally, addition of both inhibitors consistently resulted in the highest level of *BIM* mRNA expression, which was associated with the level of apoptotic cell death (Fig. 4). Since both inhibitors were successful in inducing *BIM* mRNA expression, it was suggested that the expression of BIM mRNA may be regulated by EZH2 and HDACs in TNBC cells.

BIM regulation by EZH2 and HDAC inhibitors is independent of FOXO1 expression. BIM is a well-established target gene of the transcription factor FOXO1 (27). It has been demonstrated that HDAC inhibitors can augment FOXO1 expression in phosphatase and tensin homolog (PTEN)-positive and -negative cells (28), but can only induce BIM expression by FOXO1 in PTEN-positive cancer cells (29). The expression of FOXO3, a homologue of FOXO1, is also induced by the EZH2 inhibitor

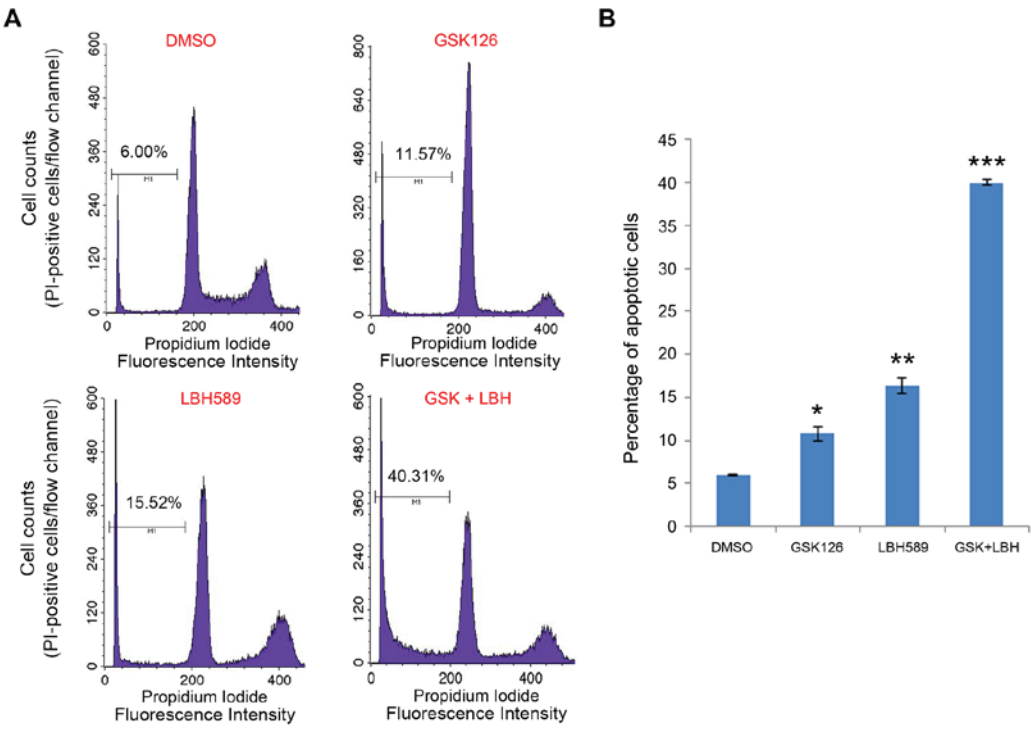

Figure 2. EZH2 and HDAC inhibitors induce apoptotic death in triple negative breast cancer cells. (A) MDA-MB-231 cells were treated with vehicle (DMSO), GSK126, LBH589 or both GSK126 and LBH589 for 24 h. Cells were harvested and stained with PI, followed by fluorescence-activated cell sorting analysis. Apoptotic cells (PI intensity <2N) were determined by CellQuest software (version 5.1; BD Biosciences, Franklin Lakes, NJ, USA). (B) The percentage of apoptotic cells in the indicated groups was determined from two replicates. Data are represented as the mean ± standard deviation (n=2). *P<0.05, **P<0.01, ***P<0.001 compared with the control (DMSO) group. EZH2, enhancer of zeste 2 polycomb repressive complex 2 subunit; HDAC, histone deacetylase; DMSO, dimethyl sulfoxide; PI, propidium iodide; N, copy number of unreplicated genome; GSK, GSK126; LBH, LBH589.

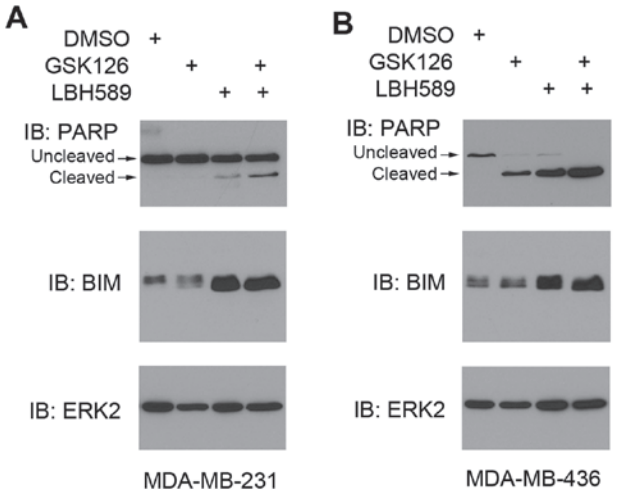

Figure 3. Treatment of triple negative breast cancer cells with EZH2 and HDAC2 inhibitors induces PARP cleavage and BIM protein expression. (A) MDA-MB-231 and (B) MDA-MB-436 cells were treated with vehicle (DMSO), GSK126, LBH589 or both GSK126 and LBH589 as indicated for 24 h. Cells were then harvested for western blot analysis using the indicated antibodies. ERK2 expression was used as a protein loading control. Similar results were obtained in two independent experiments. EZH2, enhancer of zeste 2 polycomb repressive complex 2 subunit; HDAC, histone deacetylase; PARP, poly (ADP-ribose) polymerase; BIM, B cell lymphoma-2 like 11; DMSO, dimethyl sulfoxide; ERK2, extracellular signal-related kinase 2; IB, immunoblot.

GSK126 in breast cancer 1-mutated breast cancer cells (30). It has been shown previously that MDA-MB-231 cells are PTEN-positive and MDA-MB-436 cells are negative for PTEN (31). Also, PTEN loss induces AKT activation, which phosphorylates and inhibits FOXO1 (32). Therefore, this should result in an increase in BIM expression in MDA-MB-231 cells only if HDAC and/or EZH2 inhibitor-induced BIM expression were mediated by FOXO1 upregulation. Of note, treatment with the GSK126 and LBH589 inhibitors increased BIM expression levels in both cell lines (Figs. 3 and 4). This suggested that, whereas the expression of FOXO1 may be repressed by EZH2, FOXO1 may not cause the elevated expression level of BIM observed in the present study. To investigate whether this is the case, the present study examined FOXO1 expression levels in comparison with BIM expression levels in both cancer cell lines. BIM expression levels increased upon treatment with EZH2 or HDAC inhibitor alone or together, and there was no clear indication of higher expression levels of FOXO1 in cells treated with these inhibitors, relative to mock treatment. Conversely, when treated with GSK126, FOXO1 expression was inhibited in AKT phosphorylation-positive (MDA-MB-436) and -negative (MDA-MB-231) cell lines (Fig. 5). Treatment of LBH589 alone induced FOXO1 expression in both cell lines, and was particularly pronounced in the cells with high p-AKT levels (Fig. 5). It is worth noting that increased expression of BIM (Figs. 3 and 4) was not entirely consistent with the apoptosis levels (Fig. 2). The present study also analyzed expression of p27, a different target gene of the FOXO transcription factors (33), as another functional readout to monitor the transcriptional activities of FOXO1. However, there was no positive association between FOXO1

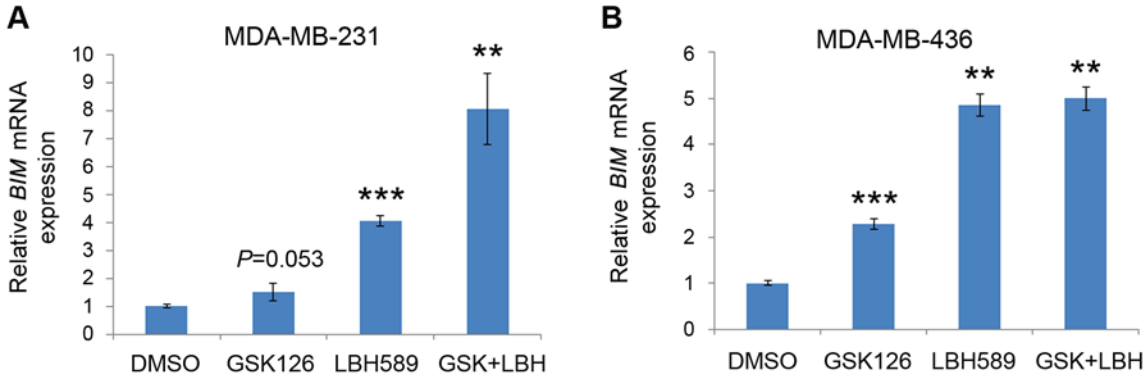

Figure 4. EZH2 and HDAC inhibitors induce *BIM* mRNA expression in triple negative breast cancer cells. (A) MDA-MB-231 and (B) MDA-MB-436 cells were treated with vehicle (DMSO), GSK126, LBH589 or both GSK126 and LBH589 as indicated for 24 h. Cells were then harvested, and *BIM* mRNA expression was analyzed by reverse transcription-quantitative polymerase chain reaction, using *GAPDH* as an internal control. All data are presented as the mean ± standard deviation (error bar) from three replicates. **P<0.01, ***P<0.001 compared with the control (DMSO) group. EZH2, enhancer of zeste 2 polycomb repressive complex 2 subunit; HDAC, histone deacetylase; *BIM*, B cell lymphoma-2 like 11; DMSO, dimethyl sulfoxide; GSK, GSK126; LBH, LBH589.

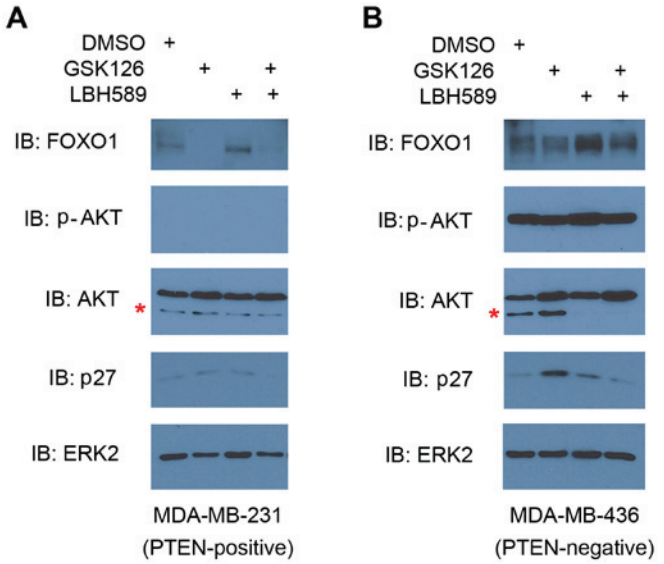

Figure 5. Effect of EZH2 and HDAC2 inhibitors on FOXO1 protein expression in triple negative breast cancer cells. (A) MDA-MB-231 and (B) MDA-MB-436 cells were treated with vehicle (DMSO), GSK126, LBH589 or both GSK126 and LBH589 as indicated for 24 h. Cells were then harvested for western blot analysis using the indicated antibodies. ERK2 expression level was used as the protein loading control. Non-specific western blotting bands are indicated by *, a phenomenon observed in HeLa cells (www.cellsignal.com/products/primary-antibodies/akt-antibody/9272?N=4294956287&Ntt=akt&fromPage=plp). Similar results were obtained in two independent experiments. EZH2, enhancer of zeste 2 polycomb repressive complex 2 subunit; HDAC, histone deacetylase; DMSO, dimethyl sulfoxide; ERK2, extracellular signal-related kinase 2; AKT, protein kinase B; p-, phosphorylated; FOXO1, forkhead box O1; PTEN, phosphatase and tensin homolog.

and p27 protein levels in PTEN-positive MDA-MB-231 and PTEN-negative MDA-MB-436 cell lines (Fig. 5). These results suggested that BIM regulation by EZH2 and HDAC inhibitors may be independent of FOXO1 expression in these TNBC cell lines.

H3K27ac in the promoter and enhancers of the BIM gene is differentially upregulated by EZH2 and HDAC inhibitors. Having ruled out the possibility of FOXO1 regulation, the present study instead hypothesized that BIM expression via EZH2 and HDAC inhibitors was directly regulated by H3K27ac levels at the promoter and/or the enhancers. Therefore, a ChIP assay was performed using anti-H3K27ac antibodies. ChIP-qPCR results demonstrated increased expression levels of H3K27ac at the *BIM* promoter when both cell lines were treated with GSK126 (Fig. 6A and B). Of note, LBH589 treatment alone resulted in a smaller increase in H3K27ac in the *BIM* promoter compared with the effect of GSK126 alone, whereas treatment with both drugs revealed no change (Fig. 6A and B), thus contradicting the increased apoptosis levels observed under these two conditions (Figs. 2 and 3). Subsequently, the present study detected an increase in H3K27ac levels at the enhancer-1 following treatment with GSK126, LBH589 or both inhibitors, and revealed that H3K27ac expression levels were highest following LBH589 treatment alone (Fig. 6A and C). At enhancer-2, the results were opposite to the effects of GSK126 or LBH589 alone or together on the *BIM* promoter (Fig. 6A and D).

Discussion

EZH2 has been identified as an important oncoprotein associated with the growth of TNBC cells (34). Thus, the present study hypothesized that treatment of TNBC cells with EZH2 inhibitors may result in apoptosis. Following initial treatment of cells with EZH2 inhibitor alone, notably, there was no marked effect on apoptosis, which lead to the hypothesis that the combination of EZH2 and HDAC inhibitors may have a greater effect on apoptosis, compared with each individual agent. The present study assumed that EZH2, a methyl-transferase enzyme, would cooperate with HDACs at the H3K27ac level. As their name implies, HDACs may remove the acetyl group and allow EZH2 to transfer a methyl group to Lys^{27} on histone H3, thereby repressing gene expression by creating a closed chromatin. Indeed, this hypothesis was supported by the observation of the present study that there was an increased pro-apoptotic effect in TNBC cells co-treated with EZH2 and HDAC inhibitors.

BIM is a pro-apoptotic protein. High expression levels of BIM were associated with the inhibition of EZH2 and HDAC

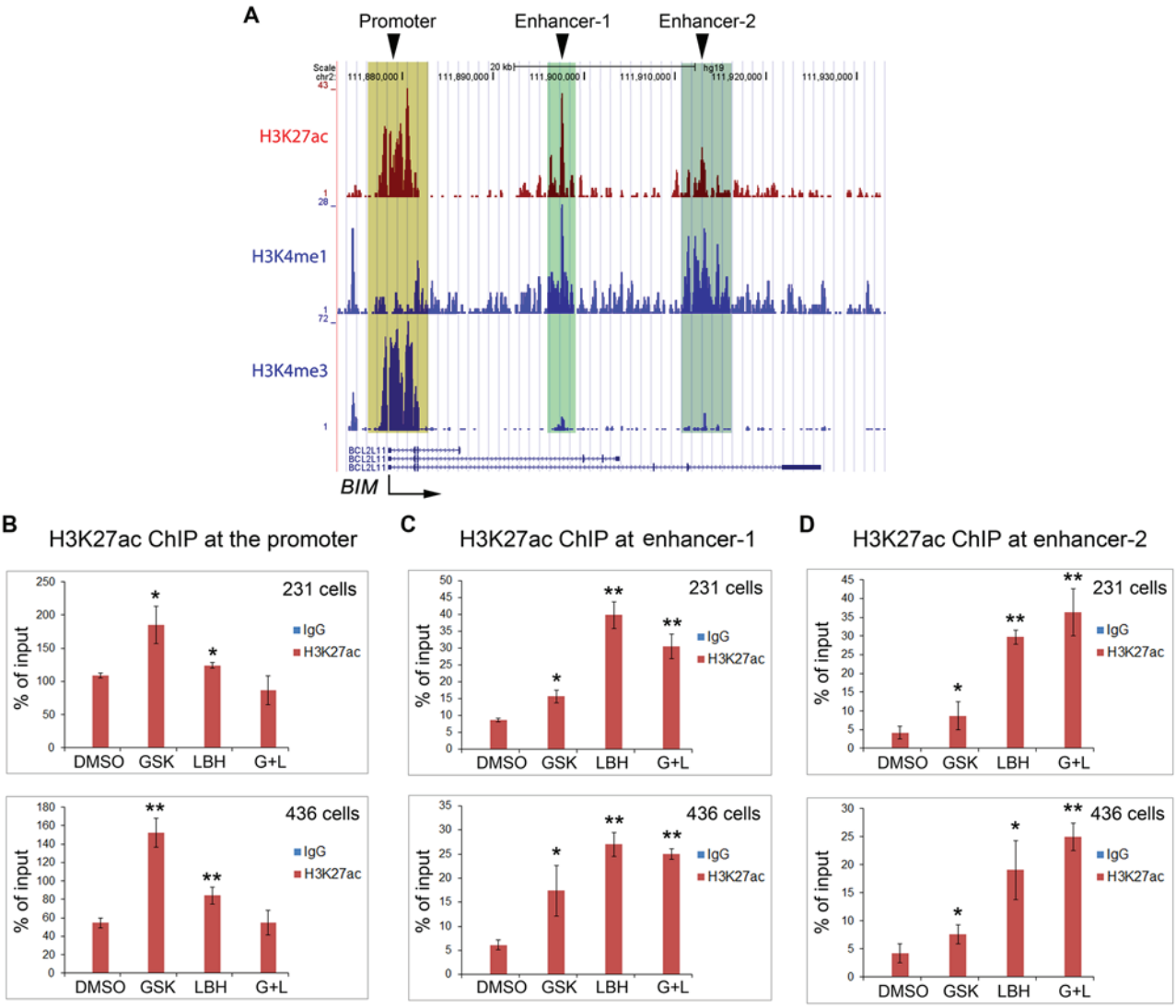

Figure 6. EZH2 and HDAC inhibitors increase H3K27ac expression levels in the *BIM* gene promoter and enhancers in triple negative breast cancer cells. (A) University of California at Santa Cruz genome browser screen shots display ChIP-seq signals of H3K27ac, the enhancer histone mark H3K4me1 and the promoter histone mark H3K4me3 obtained from the public data generated from a different cancer cell type (prostate cancer LNCaP cells). Reverse transcription-quantitative polymerase chain reaction analysis of ChIP DNA using (B) primers for the promoter, (C) putative enhancer-1 and (D) enhancer-2. DNA was immunoprecipitated by control IgG or anti-H3K27ac antibody from MDA-MB-231 and MDA-MB-436 cells treated with vehicle (DMSO), GSK126, LBH 589 or both GSK126 and LBH589. Cells were harvested for ChIP assay at 24 h after treatment. *P<0.05, **P<0.005 compared with the control (DMSO) group. H3K27me1, histone H3 Lys^{27} methylation; H3K27me3, histone H3 Lys^{27} trimethylation; H3K27ac, histone H3 Lys^{27} acetylation; EZH2, enhancer of zeste 2 polycomb repressive complex 2 subunit; HDAC, histone deacetylase; DMSO, dimethyl sulfoxide; *BIM*/*BCL211*, B cell lymphoma-2 like 11; GSK, GSK126; LBH, LBH 589; G+L, GSK126 and LBH 589; ChIP, chromatin immunoprecipitation; IgG, immunoglobulin G.

proteins. FOXO1 has been reported, in certain cellular settings, to induce BIM expression, thus presenting another possible target for treatment (35). Notably, expression of FOXO family proteins is repressed by EZH2 (30). The present study hypothesized that EZH2 inhibition elevates BIM via a mechanism of increased expression of the FOXO1 transcription factor. However, despite higher expression levels of BIM, there was a lack of a corresponding increase in the FOXO1 expression level associated with inhibition of EZH2 and/or HDAC in both TNBC cell types.

The present study assumed that both inhibitors regulated *BIM* transcription at the promoter, but repeated experiments demonstrated that this was not the case. Instead, further data established that BIM was directly regulated by the EZH2 inhibitor at the promoter, and by the HDAC inhibitor at the enhancers. Furthermore, the death of the malignant cancer cells may be more greatly affected by regulation of the enhancers compared with that of the promoter. The apoptotic effects of treatment with the EZH2 inhibitor, regulated at the promoter, were invariably lower compared with those induced by treatment with both inhibitors, and this observation was associated with increased expression levels of H3K27ac at the BIM enhances, particularly enhancer-2.

In conclusion, the results of the present study demonstrated that treating TNBC cells with an EZH2 inhibitor (GSK126) or a HDAC inhibitor (LBH589) alone produced limited effects on cell morphology, apoptotic cell death and BIM expression levels. However, a combination of both inhibitors resulted in increased tumor-killing effects which supported the hypothesis that the combination of EZH2 and HDAC inhibitors have an

increased effect on apoptosis, compared with each individual inhibitor. Additionally, the results of the present study revealed the possibility of a novel treatment strategy via additive agents.

Acknowledgements

The authors would like to thank Dr Yu Zhao (laboratory of Dr Kun Ling, the Department of Biochemistry and Molecular Biology at Mayo Clinic, Rochester, MN, USA) for his assistance with designing primers for RT-qPCR and ChIP-qPCR. The authors thank the Mayo Clinic Institutional for their support and assistance. The present study was supported in part by the National Institutes of Health/National Cancer Institute (grant no. R01CA149039).

References

1. Donepudi MS, Kondapalli K, Amos SJ and Venkanteshan P: Breast cancer statistics and markers. J Cancer Res Ther 10: 506-511, 2014.
2. DeSantis CE, Fedewa SA, Goding Sauer A, Kramer JL, Smith RA and Jemal A: Breast cancer statistics, 2015: Convergence of incidence rates between black and white women. CA Cancer J Clin 66: 31-42, 2016.
3. Schnitt SJ: Classification and prognosis of invasive breast cancer: From morphology to molecular taxonomy. Mod Pathol 23 (Suppl 2): S60-S64, 2010.
4. Callahan R and Hurvitz S: Human epidermal growth factor receptor-2-positive breast cancer: Current management of early, advanced, and recurrent disease. Curr Opin Obstet Gynecol 23: 37-43, 2011.
5. Andre F and Zielinski CC: Optimal strategies for the treatment of metastatic triple-negative breast cancer with currently approved agents. Ann Oncol 23 (Suppl 6): vi46-vi51, 2012.
6. Simon JA and Kingston RE: Mechanisms of polycomb gene silencing: Knowns and unknowns. Nat Rev Mol Cell Biol 10: 697-708, 2009.
7. Kim KH and Roberts CW: Targeting EZH2 in cancer. Nat Med 22: 128-134, 2016.
8. Simon JA and Lange CA: Roles of the EZH2 histone methyltransferase in cancer epigenetics. Mutat Res 647: 21-29, 2008.
9. Kleer CG, Cao Q, Varambally S, Shen R, Ota I, Tomlins SA, Ghosh D, Sewalt RG, Otte AP, Hayes DF, *et al*: EZH2 is a marker of aggressive breast cancer and promotes neoplastic transformation of breast epithelial cells. Proc Natl Acad Sci USA 100: 11606-11611, 2003.
10. Varambally S, Dhanasekaran SM, Zhou M, Barrette TR, Kumar-Sinha C, Sanda MG, Ghosh D, Pienta KJ, Sewalt RG, Otte AP, *et al*: The polycomb group protein EZH2 is involved in progression of prostate cancer. Nature 419: 624-629, 2002.
11. Gilbert PM, Mouw JK, Unger MA, Lakins JN, Gbegnon MK, Clemmer VB, Benezra M, Licht JD, Boudreau NJ, Tsai KK, *et al*: HOXA9 regulates BRCA1 expression to modulate human breast tumor phenotype. J Clin Invest 120: 1535-1550, 2010.
12. Wang L, Zeng X, Chen S, Ding L, Zhong J, Zhao JC, Wang L, Sarver A, Koller A, Zhi J, *et al*: BRCA1 is a negative modulator of the PRC2 complex. Embo J 32: 1584-1597, 2013.
13. Chen H, Tu SW and Hsieh JT: Down-regulation of human DAB2IP gene expression mediated by polycomb Ezh2 complex and histone deacetylase in prostate cancer. J Biol Chem 280: 22437-22444, 2005.
14. McCabe MT, Ott HM, Ganji G, Korenchuk S, Thompson C, Van Aller GS, Liu Y, Graves AP, Della Pietra A III, Diaz E, *et al*: EZH2 inhibition as a therapeutic strategy for lymphoma with EZH2-activating mutations. Nature 492: 108-112, 2012.
15. Kurmasheva RT, Sammons M, Favours E, Wu J, Kurmashev D, Cosmopoulos K, Keilhack H, Klaus CR, Houghton PJ and Smith MA: Initial testing (stage 1) of tazemetostat (EPZ-6438), a novel EZH2 inhibitor, by the Pediatric Preclinical Testing Program. Pediatr Blood Cancer 64,2017.
16. van der Vlag J and Otte AP: Transcriptional repression mediated by the human polycomb-group protein EED involves histone deacetylation. Nat Genet 23: 474-478, 1999.
17. Zhang T, Cooper S and Brockdorff N: The interplay of histone modifications-writers that read. EMBO Rep 16: 1467-1481, 2015.
18. Liu P, Kao TP and Huang H: CDK1 promotes cell proliferation and survival via phosphorylation and inhibition of FOXO1 transcription factor. Oncogene 27: 4733-4744, 2008.
19. Livak KJ and Schmittgen TD: Analysis of relative gene expression data using real-time quantitative PCR and the 2(-Delta Delta C(T)) method. Methods 25: 402-408, 2001.
20. Heintzman ND, Stuart RK, Hon G, Fu Y, Ching CW, Hawkins RD, Barrera LO, Van Calcar S, Qu C, Ching KA, *et al*: Distinct and predictive chromatin signatures of transcriptional promoters and enhancers in the human genome. Nat Genet 39: 311-318, 2007.
21. Wang D, Garcia-Bassets I, Benner C, Li W, Su X, Zhou Y, Qiu J, Liu W, Kaikkonen MU, Ohgi KA, *et al*: Reprogramming transcription by distinct classes of enhancers functionally defined by eRNA. Nature 474: 390-394, 2011.
22. Boyer LA, Lee TI, Cole MF, Johnstone SE, Levine SS, Zucker JP, Guenther MG, Kumar RM, Murray HL, Jenner RG, *et al*: Core transcriptional regulatory circuitry in human embryonic stem cells. Cell 122: 947-956, 2005.
23. Elmore S: Apoptosis: A review of programmed cell death. Toxicol Pathol 35: 495-516, 2007.
24. Riccardi C and Nicoletti I: Analysis of apoptosis by propidium iodide staining and flow cytometry. Nat Protoc 1: 1458-1461, 2006.
25. Chaitanya GV, Steven AJ and Babu PP: PARP-1 cleavage fragments: Signatures of cell-death proteases in neurodegeneration. Cell Commun Signal 8: 31, 2010.
26. Gogada R, Yadav N, Liu J, Tang S, Zhang D, Schneider A, Seshadri A, Sun L, Aldaz CM, Tang DG and Chandra D: Bim, a proapoptotic protein, up-regulated via transcription factor E2F1-dependent mechanism, functions as a prosurvival molecule in cancer. J Biol Chem 288: 368-381, 2013.
27. Gilley J, Coffer PJ and Ham J: FOXO transcription factors directly activate bim gene expression and promote apoptosis in sympathetic neurons. J Cell Biol 162: 613-622, 2003.
28. Pei Y, Liu KW, Wang J, Garancher A, Tao R, Esparza LA, Maier DL, Udaka YT, Murad N, Morrissy S, *et al*: HDAC and PI3K Antagonists Cooperate to Inhibit Growth of MYC-Driven Medulloblastoma. Cancer Cell 29: 311-323, 2016.
29. Yang Y, Zhao Y, Liao W, Yang J, Wu L, Zheng Z, Yu Y, Zhou W, Li L, Feng J, *et al*: Acetylation of FoxO1 activates Bim expression to induce apoptosis in response to histone deacetylase inhibitor depsipeptide treatment. Neoplasia 11: 313-324, 2009.
30. Gong C, Yao S, Gomes AR, Man EP, Lee HJ, Gong G, Chang S, Kim SB, Fujino K, Kim SW, *et al*: BRCA1 positively regulates FOXO3 expression by restricting FOXO3 gene methylation and epigenetic silencing through targeting EZH2 in breast cancer. Oncogenesis 5: e214, 2016.
31. Zhang J, Zhang P, Wei Y, Piao HL, Wang W, Maddika S, Wang M, Chen D, Sun Y, Hung MC, *et al*: Deubiquitylation and stabilization of PTEN by USP13. Nat Cell Biol 15: 1486-1494, 2013.
32. Nakamura N, Ramaswamy S, Vazquez F, Signoretti S, Loda M and Sellers WR: Forkhead transcription factors are critical effectors of cell death and cell cycle arrest downstream of PTEN. Mol Cell Biol 20: 8969-8982, 2000.
33. Medema RH, Kops GJ, Bos JL and Burgering BM: AFX-like forkhead transcription factors mediate cell-cycle regulation by Ras and PKB through p27kip1. Nature 404: 782-787, 2000.
34. Hussein YR, Sood AK, Bandyopadhyay S, Albashiti B, Semaan A, Nahleh Z, Roh J, Han HD, Lopez-Berestein G and Ali-Fehmi R: Clinical and biological relevance of enhancer of zeste homolog 2 in triple-negative breast cancer. Hum Pathol 43: 1638-1644, 2012.
35. Stahl M, Dijkers PF, Kops GJ, Lens SM, Coffer PJ, Burgering BM and Medema RH: The forkhead transcription factor FoxO regulates transcription of p27Kip1 and Bim in response to IL-2. J Immunol 168: 5024-5031, 2002.